Thermodynamic constraints on the petrogenesis of massif-type anorthosites and their parental magmas

Fred, Riikka Maria

2022-08

Contents lists available at ScienceDirect

LITHOS

Thermodynamic constraints on the petrogenesis of massif-type anorthosites and their parental magmas

Riikka Fred [a],[*], Jussi S. Heinonen [a], Aku Heinonen [a], Wendy A. Bohrson [b]

[a] *Department of Geosciences and Geography, University of Helsinki, Gustaff Hältströmin katu 2, PO Box 64, 00014 Helsinki, Finland*
[b] *Department of Geology and Geological Engineering, Colorado School of Mines, 1516 Illinois St., Golden, CO 80401, United States of America*

ARTICLE INFO

ABSTRACT

Development of computational modeling tools has revolutionized studies of magmatic processes over the last four decades. Their refinement from binary mixing equations to thermodynamically controlled geochemical assimilation models has provided more comprehensive and detailed modeling constraints of an array of magmatic systems. One of the questions that has not yet been vigorously studied using thermodynamic constraints is the origin of massif-type anorthosites. The parental melts to these intrusions are hypothesized to be either mantle-derived high-Al basaltic melts that undergo crustal contamination or monzodioritic melts derived directly from lower crust. On the other hand, many studies suggest that the monzodioritic rocks do not represent parental melts but instead represent crystal remnants of residual liquids left after crystal fractionation of parental melts. Regardless of the source or composition, magmas that produce massif-type anorthosites have been suggested to have undergone polybaric (~1000–100 MPa) fractional crystallization while ascending through the lithosphere.

We conducted lower crustal melting, assimilation-fractional crystallization, and isobaric and polybaric fractional crystallization major element modeling using two thermodynamically constrained modeling tools, the Magma Chamber Simulator (MCS) and rhyolite-MELTS, to test the suitability of these tools and to study the petrogenesis of massif-type anorthosites. Comparison of our models with a large suite of whole-rock data suggests that the massif-type anorthosite parental melts were high-Al basalts that were produced when hot mantle-derived partial melts assimilated lower crustal material at Moho levels. These contaminated basaltic parental magmas then experienced polybaric fractional crystallization at different crustal levels (~40 to 5 km) producing residual melts that crystallized as monzodioritic rocks. Model outcomes also support the suggestion that the cumulates produced during polybaric fractional crystallization likely underwent density separation, thus producing the plagioclase-rich anorthositic rocks. The modeled processes are linked to a four-stage model that describes the key petrogenetic processes that generate massif-type anorthosites. The presented framework enables further detailed thermodynamic and geochemical modeling of individual anorthosite intrusions using MCS and involving trace element and isotope constrains.

1. Introduction

The development of geochemical and thermodynamic modeling tools has enabled unprecedented advances in studying magmatic systems (e.g., Heinonen et al., 2021). The humble beginnings of binary mixing calculations led to assimilation-fractional crystallization equations (AFC; e.g., Taylor, 1980; DePaolo, 1981), which were later augmented with rudimentary energy constraints (EC-AFC; Bohrson and Spera, 2001, 2007; Spera and Bohrson, 2001), and, finally, with predictions of phase equilibria in the Magma Chamber Simulator (MCS;

Bohrson et al., 2014, 2020). The MCS can be used to model simultaneous magma crystallization, magma recharge (and mixing), and crustal assimilation in an evolving multicomponent-multiphase open magmatic system (Bohrson et al., 2014, 2020). These advancements have provided more comprehensive and detailed petrogenetic studies of magmatic systems of diverse composition, geotectonic affiliation, and age (e.g., Borisova et al., 2017; Heinonen et al., 2019; Iles and Heinonen, 2022; Kärenlampi et al., 2021).

Anorthosites and their associated less feldspathic lithologies (i.e., anorthositic rocks) exhibit simple modal composition and mainly consist

* Corresponding author.
E-mail address: riikka.fred@helsinki.fi (R. Fred).
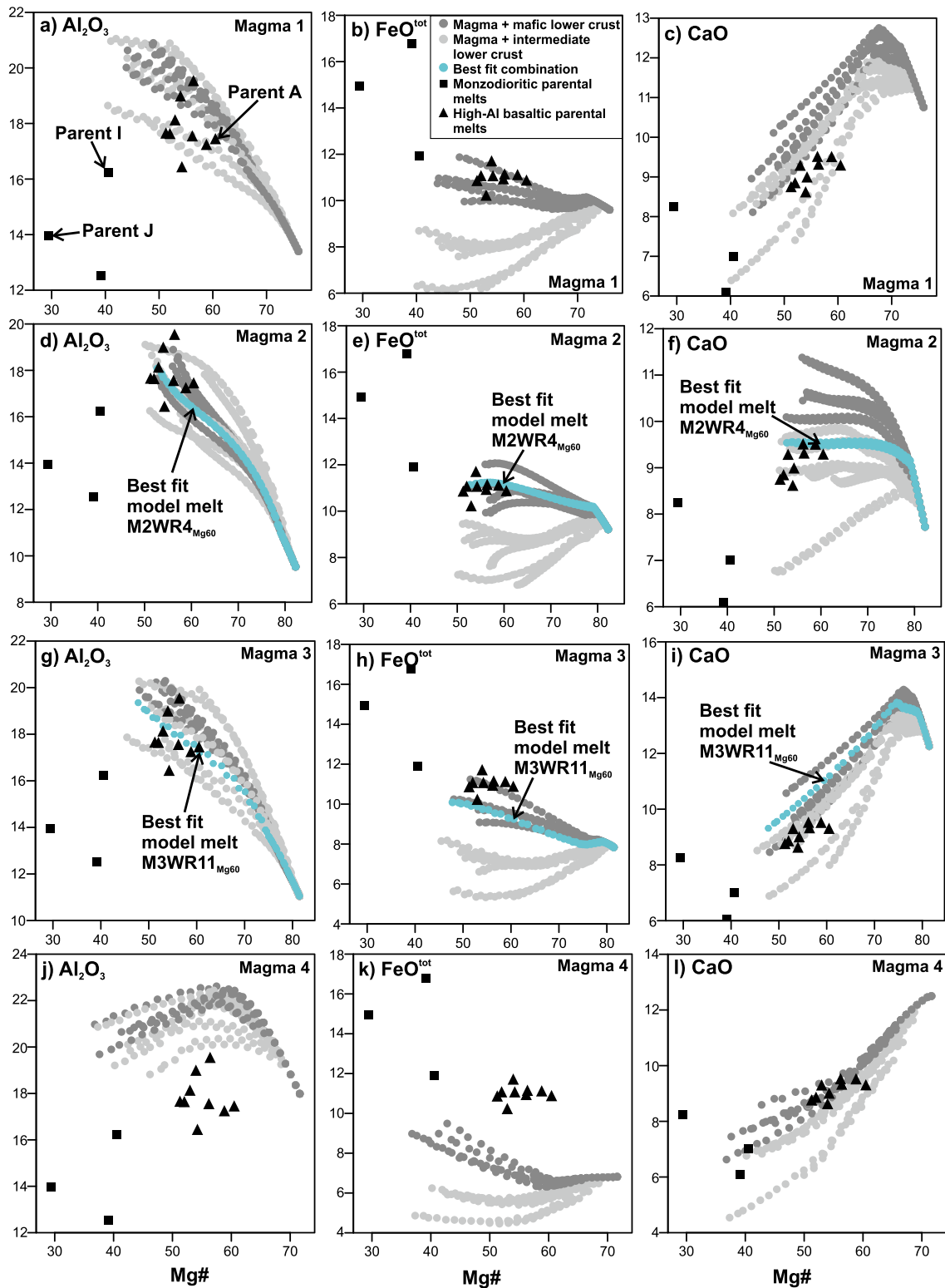
Fig. 3. Comparison of selected LLDs (Mg# versus oxide in wt%) produced by MCS-AFC simulations (Table 1) of M1 (a–c), M2 (d–f), M3 (g–i), and M4 (j–l) with previously suggested 11 high-Al basaltic and monzodioritic massif-type anorthosite parental melts (parents A–K). Best fit magma-wallrock combinations (M2WR4$_{Mg60}$ and M3WR11$_{Mg60}$) are highlighted with turquoise and Parents A, I, and J used in FC models are indicated in plot a. See section 3.2 for details. (For interpretation of the references to colour in this figure legend, the reader is referred to the web version of this article.)

only iFC model results for M3WR11$_{Mg60}$ and monzodioritic parent I are illustrated in the manuscript (Figs. 4–7). These compositions represent end-members in our modeling and were thus chosen to be shown here – the rest of the modeling results (for M2WR4$_{Mg60}$, high-Al basaltic parent

A, and monzodioritic parent J melts) are illustrated in Supplementary material E.

The global data of monzodioritic rocks show wide variation for some oxides, but the iFC simulations for model melts M2WR4$_{Mg60}$ and
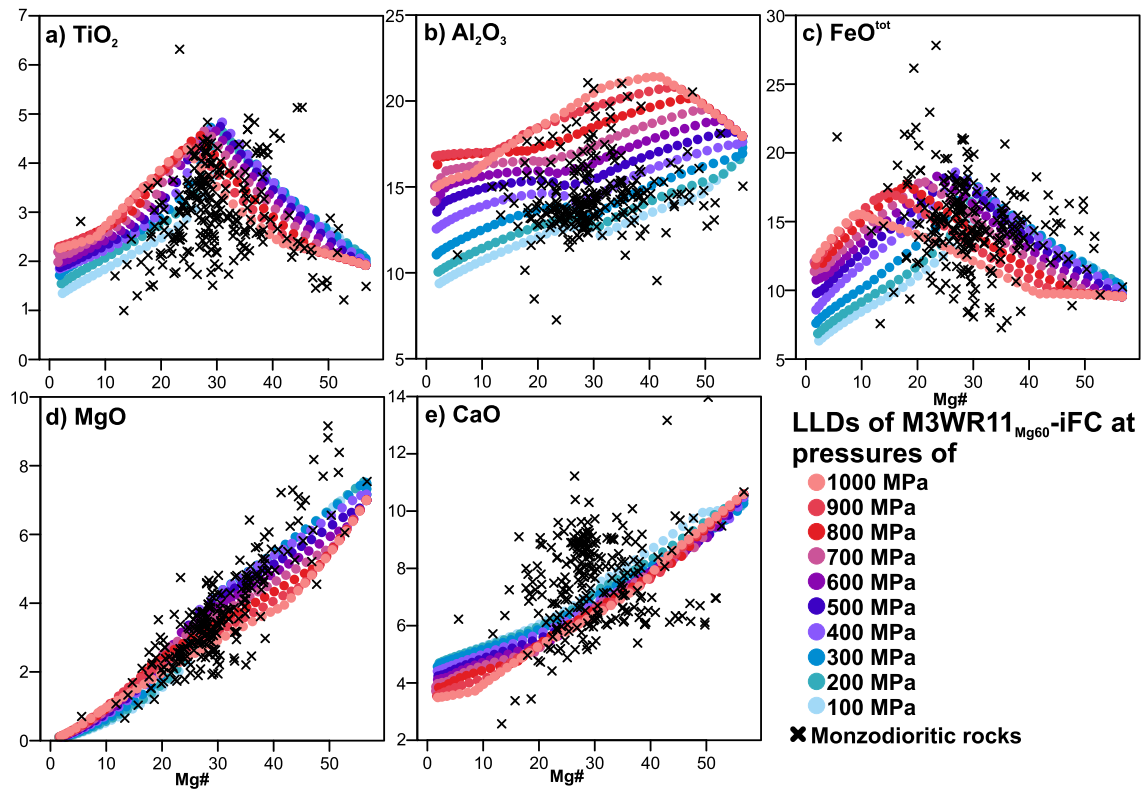
Fig. 4. Selected LLDs (Mg# versus oxide in wt%) produced in closed-system isobaric fractional crystallization simulations using M3WR11 model melt after MCS-AFC (40% of assimilation, Mg# ~ 60, Table 1) compared to compositional evolution trends of global data set of monzodioritic rocks (Fred et al., 2020 and references therein; Supplementary material A) . See section 3.3 for details.

Fig. 5. Selected LLDs (Mg# versus oxide in wt%) produced in closed-system isobaric fractional crystallization simulations using monzodioritic parent I (Table 1) compared to compositional evolution trends of global data set of monzodioritic rocks (Fred et al., 2020 and references therein; Supplementary material A) . See section 3.3 for details.

Fig. 6. Selected incremental cumulate compositions (Mg# versus oxide in wt%) produced in closed-system isobaric fractional crystallization simulations using M3WR11$_{Mg60}$ model melt after MCS-AFC compared to a data set of anorthositic rocks from the Adirondacks suite and Ahvenisto Complex (Supplementary material A). See section 3.3 for details.

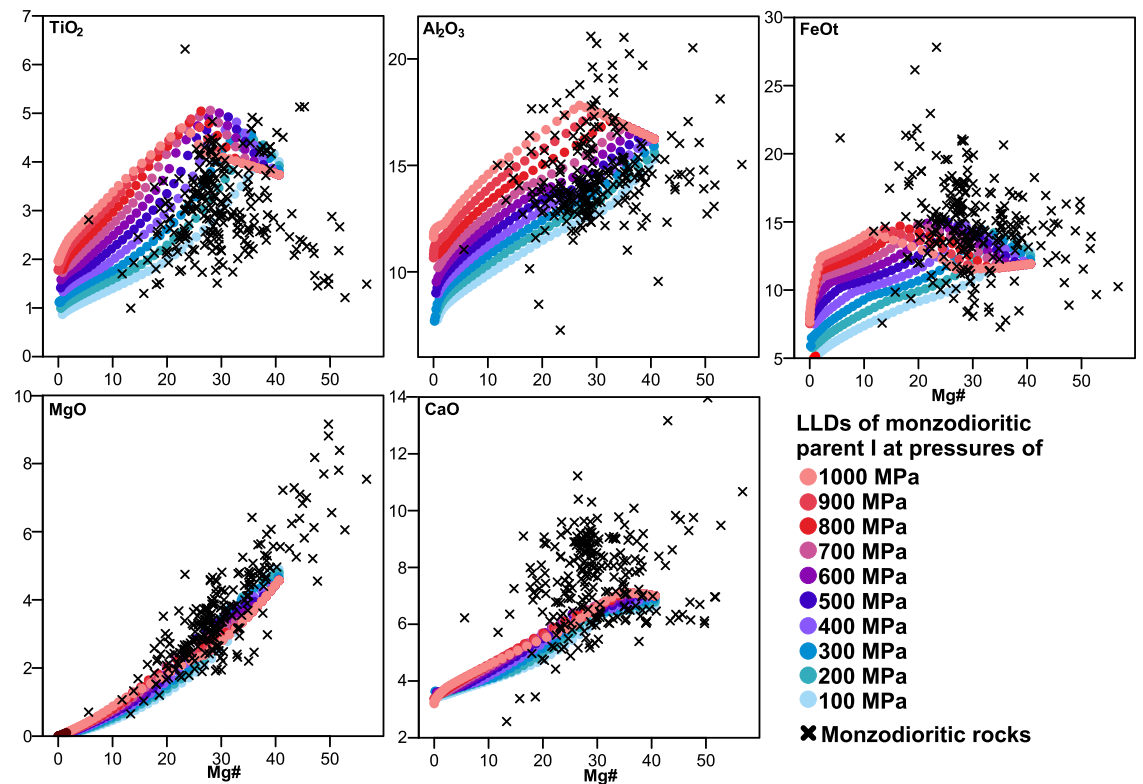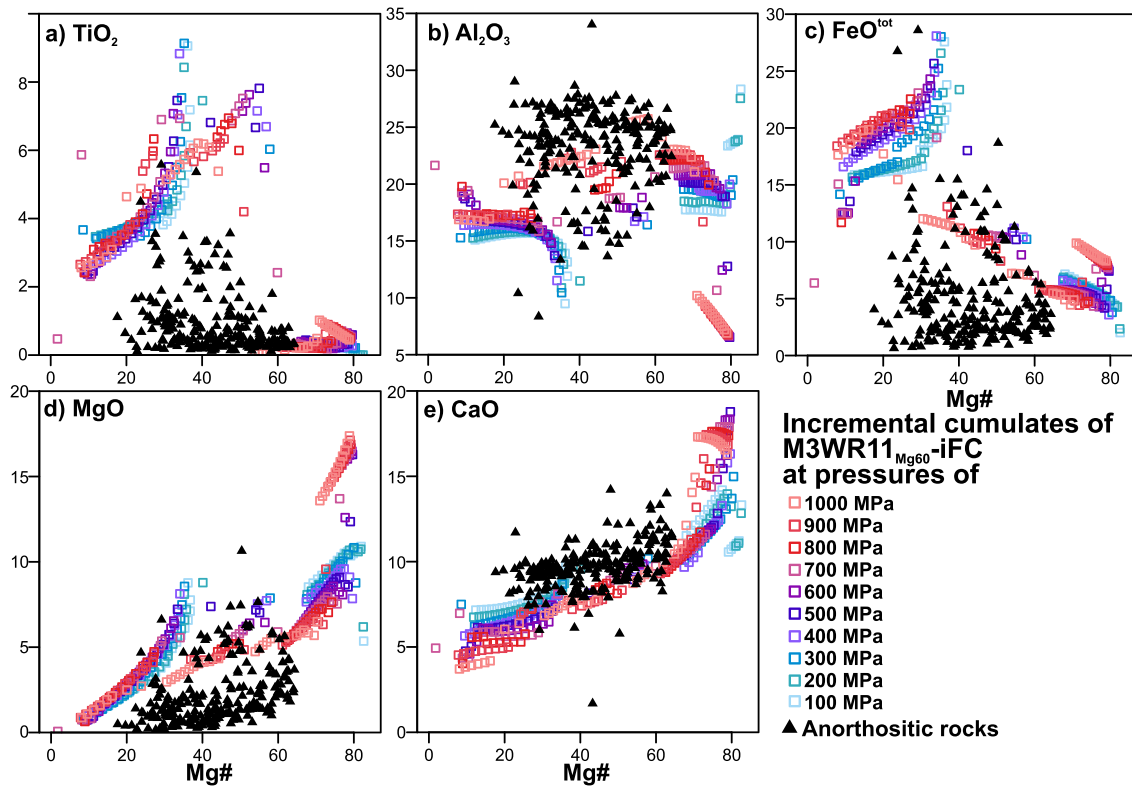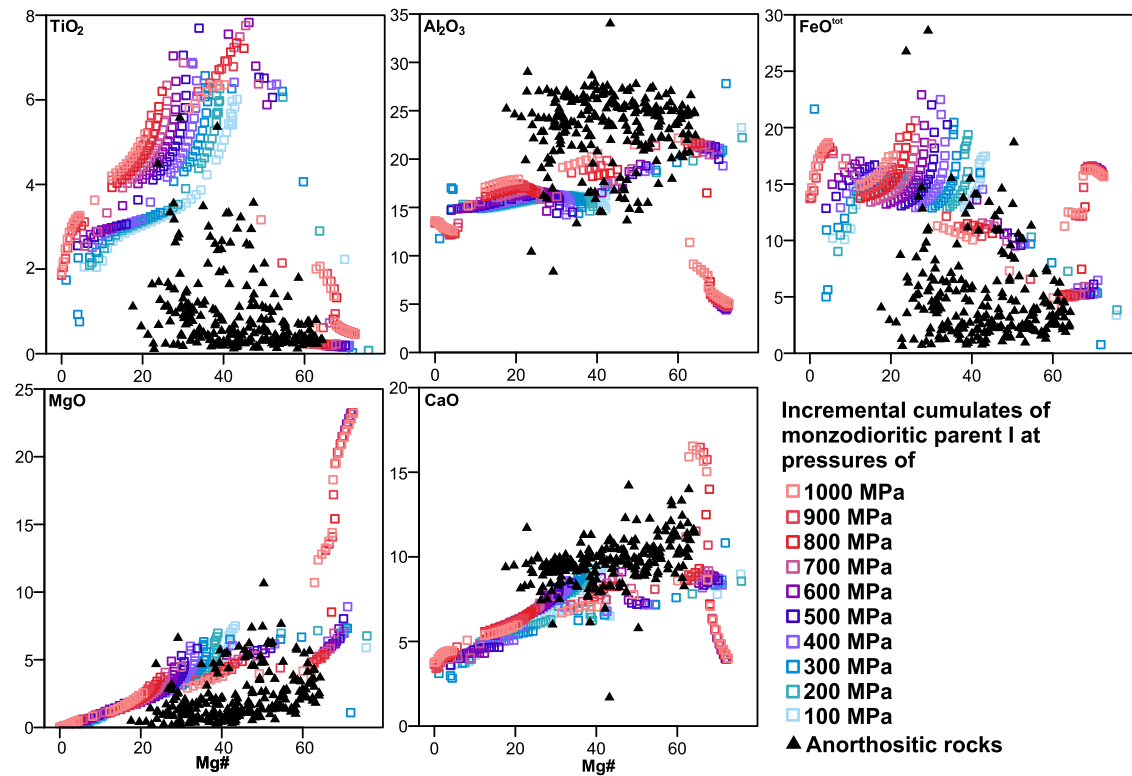**Fig. 7.** Selected incremental cumulate compositions (Mg# versus oxide in wt%) produced in closed-system isobaric fractional crystallization simulations using monzodioritic parent I to a data set of anorthositic rocks from the Adirondacks suite and Ahvenisto Complex (Supplementary material A). See section 3.3 for details.

M3WR11$_{Mg60}$, and the previously suggested high-Al basaltic parent A, show similar trends with the main monzodioritic rock trends for many oxides (Fig. 4; Supplementary material E). For some oxides, such as CaO, the results are inconclusive. For example, model melt M3WR11$_{Mg60}$ produces somewhat higher Na$_2$O and lower CaO contents compared to the monzodioritic rocks. The Al$_2$O$_3$ content of the monzodioritic rocks shows wide variation (~7–22 wt%), but the entire range is covered well with the iFC models conducted at different pressures (Fig. 4b). This indicates that crystallization pressure may play a role in the compositional variation of the monzodiorites.

Simulations using the previously suggested monzodioritic parental magma compositions I and J do not cover the entire range of monzodioritic rock data (Fig. 5; Supplementary material E). The LLDs derived from the primitive monzodioritic parent I, however, show similar trends with more evolved monzodioritic rocks in terms of, for example, TiO$_2$, Al$_2$O$_3$, MgO, and K$_2$O (Fig. 6). On the other hand, the models show higher SiO$_2$ and Na$_2$O and lower FeO^{tot} and CaO trends compared to the natural monzodioritic trends.

In addition to major oxide trend comparisons, we also compiled and compared the mineral modes and mineral chemistries of the simulations. In the M2WR4$_{Mg60}$-iFC simulations >600 MPa, clinopyroxene is the most abundant phase. In contrast, plagioclase is the most abundant mineral to crystallize in the simulations <600 MPa and the amount increases from 40 wt% at 1000 MPa to ~55 wt% at 100 MPa (Table 2). Olivine also occurs as a major phase. In M3WR11$_{Mg60}$-iFC simulations, plagioclase is the most abundant phase at all pressures (40–60%, 1000–100 MPa, respectively), and the plagioclase/clinopyroxene ratio increases with decreasing pressure; their amounts are almost equal at 1000 MPa (Table 2). The plagioclase/clinopyroxene ratios are similar in simulations using the previously suggested high-Al basaltic parent A. With respect to end-member pressures of 1000 and 100 MPa, the plagioclase An-content ranges from An$_{50-23}$ to An$_{78-61}$ in M2WR11$_{Mg60}$-iFC simulations, from An$_{78-65}$ to An$_{33-25}$ in M3WR11$_{Mg60}$-iFC simulations, and An$_{77-70}$ to An$_{48-22}$ in simulations using the high-Al basaltic parent A; the highest An-contents are found at the lowest pressures (Table 2). The range of plagioclase An-contents in the simulations are in the global range of plagioclase compositions (An$_{30-90}$) of massif-type anorthosites (Ashwal and Bybee, 2017).

In the simulations using monzodioritic parents I and J, plagioclase is the first phase to crystallize at lower pressures (100–300 MPa; Table 2). In the simulations using the primitive monzodioritic parent I, the amount of accumulated plagioclase is 60 wt% at 100 MPa compared to ~50 wt% at 1000 MPa (Table 2). In the simulations using the evolved monzodioritic parent J, the amount of plagioclase increases from 45 wt% at 1000 MPa to 50 wt% at 100 MPa (Table 2). Other major phases to crystallize are clinopyroxene (35–15 wt% relative to decreasing pressure in parent I simulations and 35–25 wt% in parent J simulations) and spinel (15–5 wt% in parent I simulations and 20–10 wt% in parent J simulations). The An-content evolves from ~An$_{40-45}$ to An$_{20}$ at 1000 MPa and from ~An$_{60}$ to An$_{20}$ at 100 MPa in simulations using parent I and J.

The second hypothesis we tested asserts that the cumulates formed by iFC produce the anorthositic rocks. The incremental cumulate compositions of the iFC models were compared to anorthositic cumulate compositions from the Adirondacks and Ahvenisto complexes (examples derived from M3WR11$_{Mg60}$ and monzodioritic parent I shown in Figs. 6 and 7, respectively; complete results in Supplementary material F). The modeled incremental cumulate compositions show the composition of the cumulates removed from the magma at each temperature step during the iFC simulations. The wide compositional variation of the modeled cumulates reflects the changes in what phases are crystallizing at each specific temperature step. For example, the low Al and high Mg contents of the earliest cumulates reflects that pyroxene is the only crystallizing phase (Figs. 6 and 7). The compositional leaps in some oxides, thus, simply reflect the appearance/disappearance of phases in the crystallizing assemblage.

Based on of visual inspection, the incremental cumulate compositions of the iFC simulations show wide variations due to the reasons given above, and therefore the comparison of the visual fits with the natural anorthositic cumulates should concentrate on comparing to rocks with similar phase assemblages. The incremental model cumulates derived from M3WR11$_{Mg60}$ parental melt typically show higher TiO$_2$, FeO^{tot}, and MgO and lower SiO$_2$, Na$_2$O, and K$_2$O in simulations compared to natural anorthositic cumulates (Fig. 6). Al$_2$O$_3$ and CaO of the simulations produce the best fit with natural samples, although still somewhat lower than observed. In simulations using the primitive monzodioritic parent I, the incremental cumulate compositions are more similar to the natural samples in general, with Na$_2$O showing the best fit (Fig. 7). Al$_2$O$_3$ and CaO contents are somewhat lower than in the simulations using model melt M3WR11$_{Mg60}$ (Figs. 6 and 7).

3.4. Polybaric fractional crystallization modeling and comparison to the monzodioritic rocks

Finally, we also studied the effects of polybaric fractional crystallization for the model melts M2WR4$_{Mg60}$ and M3WR11$_{Mg60}$ and high-Al basaltic parental magma A using rhyolite-MELTS. The models were run from the liquidus temperature with 5 °C temperature decrement using different starting pressures (1000 and 500 MPa) and dP/dT (13–26). All of these pFC models were compared to the global dataset of monzodioritic rocks to test the hypothesis that these rocks represent residual melts compositions left after anorthosite fractionation (e.g., Ashwal, 1982; Bybee et al., 2015; Emslie et al., 1994; Fred et al., 2020; Heinonen et al., 2010; McLelland et al., 1994; Mitchell et al., 1996).

In Fig. 8, the Al$_2$O$_3$ content of the pFC simulations was chosen for more detailed examination, because Al$_2$O$_3$ shows wide variation in the monzodioritic rocks and in the iFC simulations at different pressures (Fig. 4). All the polybaric simulations that cover the entire pressure range used in the iFC simulations (1000–100 MPa) give higher Al$_2$O$_3$ contents compared to the main monzodioritic trend (Fig. 8). In the simulations where the previously suggested high-Al basaltic parent A was used, the simulation with a pressure decrease from 500 to 120 MPa gives the best fit (Fig. 8a). The best fit for the simulations using MCS-AFC model melts was produced by the M3WR11$_{Mg60}$-pFC simulations with a pressure decrease from 500 to 210 MPa (Fig. 8c).

Cumulate compositions for the complementary pFC simulations were not calculated, but the crystallizing phases are similar to those of the iFC simulations. In the simulations using high-Al basaltic parent A, the major crystallizing phases are plagioclase, clinopyroxene, orthopyroxene, and olivine and in the simulations using the model melts M2WR4$_{Mg60}$ and M3WR11$_{Mg60}$ the major crystallizing phases are plagioclase, clinopyroxene, olivine and spinel. Similar to the iFC models, plagioclase and clinopyroxene are the most abundant phases and their ratio varies as a function of pressure and temperature range.

4. Discussion

We used different thermodynamically constrained modeling approaches (lower crustal melting, AFC, and isobaric and polybaric FC) to study some of the hypotheses presented for the petrogenesis of massif-type anorthosites: 1) production of the anorthosite parental melts by direct melting of the lower crust, 2) production of the anorthosite parental melts by assimilation-fractional crystallization, and 3) production of the anorthositic cumulates and monzodioritic rocks by fractional crystallization during magma ascent through the crust (1000–100 MPa; Fig. 1).

4.1. Composition and source of the anorthosite parental magmas

Our partial melting modeling conforms with the hypothesis that production of melts similar to the previously suggested high-Al basaltic parental magma compositions of massif-type anorthosites would require
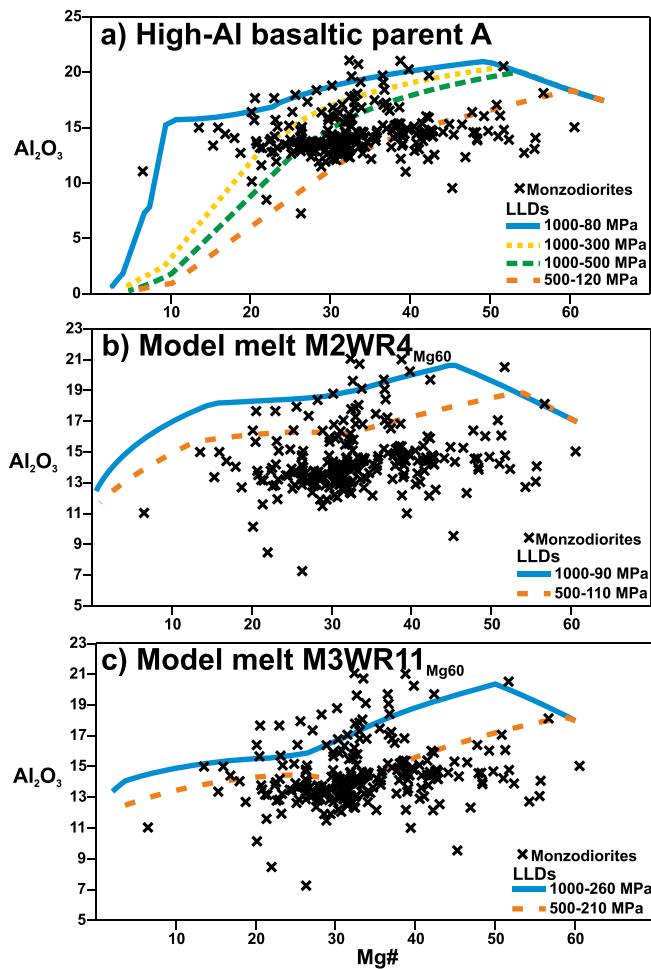
Fig. 8. Examples of LLDs produced in pFC simulations using a) previously suggested high-Al basaltic parent A and model melts b) M2WR4$_{Mg60}$ and c) M3WR11$_{Mg60}$ after MCS-AFC at Mg# ~ 60 (Table 1) compared to the monzodioritic data set (Fred et al., 2020 and references therein). See section 3.4 for details.

the lower crustal material to melt almost completely or completely (>70 wt%; Fig. 2; Table 2). For such high-degree of melting, ambient temperatures of 1240–1380 °C at 1000 MPa would be required, which is unfeasible without simultaneous partial melting of the mantle taking place. For example, experimental solidus temperatures of 1190–1270 °C at 1000 MPa for different ambient dry peridotitic mantle compositions have been documented (Kiefer et al., 2015). Also, the volume of crust needed to produce the parental magmas of suites such as the Nain Plutonic Suite would be enormous (see Bybee et al., 2014b), and melting that much lower crust without compensatory melt input from the mantle would have a dramatic effect on the stability of the crust (Ashwal and Bybee, 2017).

In contrast, the results of the MCS-AFC models suggest that melts with similar compositions to the previously inferred high-Al basaltic compositions can be produced by crustal contamination of hot primitive mantle melts. The (initial) liquidus temperatures of the melts at 1000 MPa (1360–1600 °C) suggest that the mantle must have been anomalously hot – ambient upper mantle temperatures in the early Proterozoic were potentially only 100 °C higher than today (Ganne and Feng, 2017). The high mantle temperature implied by our modeling could be explained by a mantle plume or warming of the mantle by supercontinent insulation, which can lead to an increase of mantle temperature in excess of 100 °C (Coltice et al., 2007, 2009). Indeed, many massif-type anorthosites are temporally associated with supercontinents, and a

connection between supercontinent closing and opening cycles with massif-type anorthosites has been suggested (e.g., Mukherjee and Das, 2002). Such high temperatures promote melting of the mantle and thus could explain the large amounts of molten material needed to produce the largest AMCG suites. A key outcome of our modeling is that the amount of melt left after the AFC at 1000 MPa is still high (generally ~70%), and, thus, can provide the required mass to generate the observed large volumes of anorthositic rocks. The success of the MCS-AFC models strongly suggests that the source for the parental magmas of massif-type anorthosites is the mantle with significant mass contributions also from assimilation of lower crustal material. Producing the parental melts by AFC also addresses for the aforementioned stability issue of the direct lower crustal melting hypothesis, since the mass loss from the lower crust is replaced by the crystallizing cumulates.

Based on high-pressure experimental work and previously published rudimentary FC and AFC calculations, it has been suggested that crystallization of mantle-derived melts with or without assimilation cannot produced either the high-Al basaltic or monzodioritic melts and that they can only be produced by melting of crustal material (Longhi, 2005; Longhi et al., 1999). These studies did not consider extensive assimilation of the lower crust, however. As stated above, our thermodynamic modeling suggest that high-Al basaltic melts can indeed be produced by AFC at high pressures and on many occasions, this requires large amount of assimilation of lower crust. The thermodynamic models do not exclude the possibility of producing the high-Al basaltic melts by melting lower crustal material only, but this is considered improbable for the reasons stated above. Nevertheless, assimilation plays major role in the early stages during anorthosite petrogenesis, and we emphasize the important role of lower crustal melting in production of the observed compositions in massif-type anorthosite suites.

The LLDs produced in our MCS-AFC models point toward assimilation with mafic rather than felsic lower crustal material (Fig. 3), which is in contradiction to the suggestions of Ashwal and Bybee (2017), who speculate that the assimilants would mostly be of granitic compositions. As is well known, the crust is compositionally heterogeneous and when deciphering the parental magma compositions for individual suites, the composition of the assimilant needs to be investigated in the light of the case-specific crustal architecture. In addition to the heterogeneity provided by the composition of the crust, the amount of assimilation will also vary, based on a number of factors (e.g., geothermal gradient and crustal composition), which naturally affects the compositional evolution of the melts. This is also evidenced by our models where the amount of assimilation generally varies from 20 to 70% in simulations using different magma-wallrock combinations.

The trace element and isotope compositions are specific for each anorthosite suite and their treatment is thus outside of the scope of this study. They have also played an important role in the debate on the source for the anorthosite parental magmas (e.g., Bybee et al., 2014a; Hannah and Stein, 2002; Heinonen et al., 2010, 2015; Mitchell et al., 1995; Schiellerup et al., 2000) and generally support our suggestion that the parental magmas to anorthositic rocks are mantle-derived melts that have undergone lower crustal contamination. Whereas isotope data rather clearly suggest a mantle origin for some suites (e.g., Bybee et al., 2014a; Heinonen et al., 2010; Mitchell et al., 1995), some other systems show strong crustal signatures, which has led to the hypotheses of lower crustal origin (e.g., Schärer et al., 1996; Schiellerup et al., 2000). Furthermore, introduction of energy constraints into the AFC models and the ability to model partial melting of the wallrock, has shown that mantle-derived magmas can inherit strong crustal radiogenic isotope signatures even with low amounts (<20%) of assimilation (e.g., Fowler et al., 2004; Heinonen et al., 2016). Assimilation of crustal material by mantle-derived primitive melts could thus result in crust-like isotopic signatures and varying amounts of crustal assimilation can lead to similar or much larger variations in isotopic data compared to those resulting from source heterogeneity (Fowler et al., 2004; Hannah and Stein, 2002). Our MCS-AFC models suggest that the amount of

assimilation could be up to 70 wt% of mafic lower crustal material and, hence, would lead to a strong crustal trace element and radiogenic isotopic signatures.

Our MCS-AFC models further suggest that the massif-type anorthosite parental magma compositions are represented by the previously suggested high-Al basaltic and not monzodioritic compositions (Figs. 2 and 3). Further examination of melt evolution by fractional crystallization of these parents suggests that the LLDs produced in FC simulations show similar trends in some oxides with the monzodioritic rocks, and, thus, that the monzodioritic rocks represent derivatives of the high-Al basaltic parental magmas, i.e., residual melt compositions (Figs. 4 and 5). The global monzodioritic dataset, however, shows wide compositional variation. This and the evolution of the monzodioritic magmas are discussed in more detail in the following section. The level of exposure in different suites varies, and hence in some intrusions only more evolved rocks are observed. The compositions of the parental melts evolves continuously during the (assimilation-) fractional crystallization of the anorthositic cumulates, and hence the melts that the more evolved anorthositic cumulates crystallized from, most likely were already more similar in composition to the primitive monzodioritic rocks than to the high-Al basaltic parental compositions.

4.2. Origin of the monzodioritic rocks: Implications for crystallization and accumulation processes in different anorthosite suites

We examined the geochemistry of monzodioritic rocks and the evolution of the associated melts by comparing the pressure-dependent Al_2O_3 contents of some of the individual intrusions included in the global data set (Fig. 9). In several cases, the monzodioritic whole-rock data form a rather concise trend, but in others the data are more dispersed. In the Ahvenisto complex and Korosten intrusion, most of the monzodioritic rocks form a trend that closely follows the modeled LLDs at lower pressures (<500 MPa), whereas few samples plot on LLDs at higher pressures (Fig. 9). In the Laramie intrusion and especially in the

Adirondacks data set, the monzodioritic rocks are spread over the LLDs of the whole pressure range (100–1000 MPa), whereas the monzodioritic rocks of the Norwegian intrusions plot on LLDs at lower pressures (<500 MPa, Fig. 9).

There are several options that could explain the dispersion of the data from these whole-rock samples, including polybaric crystallization of the monzodioritic rocks or accumulation of plagioclase; that is, some of the samples may actually represent monzodioritic or anorthositic cumulates or at least contain some cumulus plagioclase (see Fred et al., 2020). Examination of Figs. 5, 8, and 9 shows that 90% of the monzodiorite data plot on or close to the simulated LLDs at lower pressures (100–500 MPa). This indicates that the monzodioritic rocks could represent the residual melt compositions left after the fractionation of anorthositic cumulates at relatively low pressures (<500 MPa).

In Fig. 9, the monzodioritic rocks are plotted with LLDs produced in iFC models (100 and 1000 MPa) together with plagioclase accumulation trends and incremental cumulate compositions with Mg# < 70 of M3WR11$_{Mg60}$-iFC (100–1000 MPa). As stated for the whole monzodioritic data set in section 3.4, the main trend of the monzodioritic rocks plots close to the lower pressure (500–200 MPa) polybaric FC trend, indicating crystallization at lower pressures. The samples with higher Al_2O_3 and CaO of individual intrusions are in the range of plagioclase accumulation trends, and also fit quite well with incremental cumulate compositions (Fig. 9), indicating that these samples more likely represent cumulate varieties of the monzodioritic rocks or monzodioritic rocks with cumulate plagioclase or even in some cases anorthositic cumulates, rather than fine-grained monzodioritic rocks of near-melt compositions crystallized at higher pressures. Thus, the Adirondacks dataset might include more samples with cumulate plagioclase, which explains the dispersed data. Although, as mentioned in section 1, there are several other hypothesis presented for the origin of the monzodioritic rocks based on the modeling results and discussion shown here together with previous contributions (e.g., Ashwal, 1982; Morse, 1982; Duchesne, 1984; Owens and Dymek, 1992; Emslie et al., 1994;
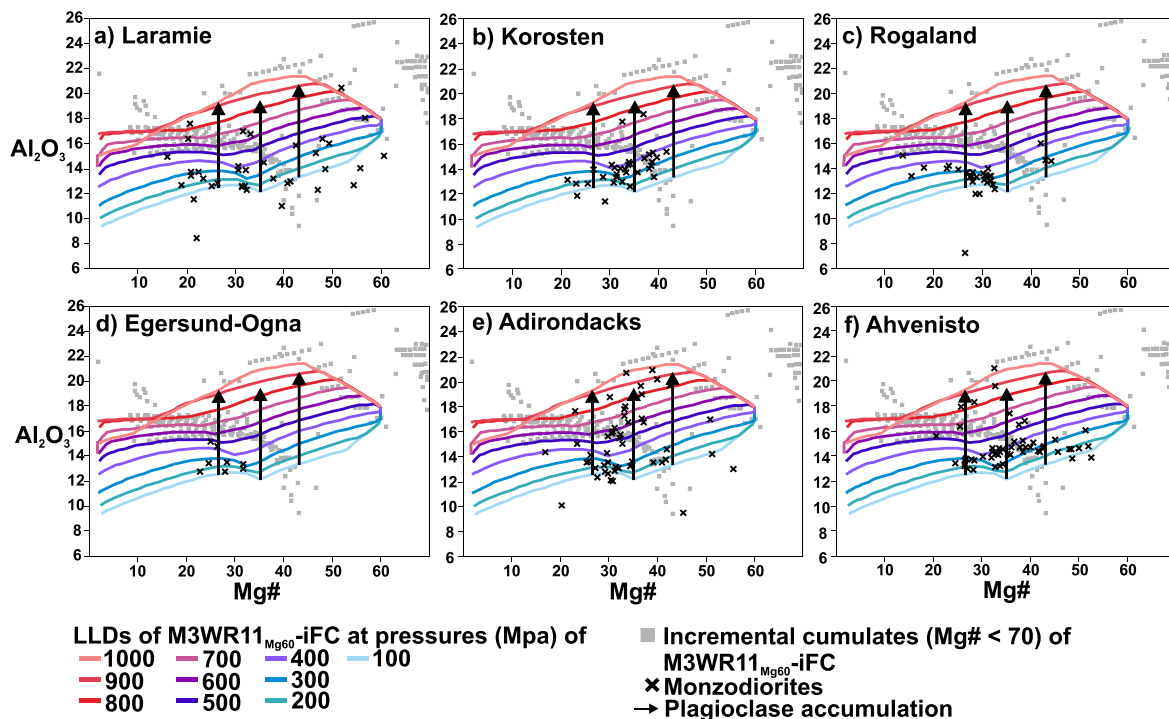
Fig. 9. Mg# versus whole-rock Al_2O_3 (wt%) of monzodioritic rocks of individual AMCG suites from a) Laramie, Wyoming, USA, b) Korosten, Ukraine, c) Rogaland, Norway, d) Egersund-Ogna, Norway, e) Adirondacks mountains, New York, USA, and f) Ahvenisto complex, Finland compared to LLDs of M3WR11$_{Mg60}$-iFC (1000–100 MPa), incremental cumulate compositions (Mg# <70) of M3WR11$_{Mg60}$-iFC (1000–100 MPa), and calculated plagioclase accumulation trends. The added plagioclase composition is plagioclase model compositions at the step corresponding to Mg# of the M3WR11$_{Mg60}$-iFC simulation. See section 4.2 for details.

McLelland et al., 1994; Mitchell et al., 1996; Vander Auwera et al., 1998; Dymek and Owens, 2001; Markl, 2001; Heinonen et al., 2010; Bybee et al., 2015, Fred et al., 2020) the residual melt hypothesis is the most propitious.

One of the main arguments against the residual melt hypothesis is the lack of negative Eu-anomalies in some of the monzodioritic rocks, for example primitive monzodioritic parent I, which suggest the melts have not gone through plagioclase fractionation. However, not all of the monzodioritic rocks lack the negative Eu-anomalies and many of them show at least small negative Eu-anomalies (e.g., Owens et al., 1993; Mitchell et al., 1996; Duchesne et al., 2017). For example, in the Ahvenisto complex, only the most primitive monzodioritic rocks lack Eu-anomalies while the more evolved ones show a negative Eu-anomaly, which is expected due to removal of plagioclase from the melts (Fred et al., 2020). Many of the monzodioritic rocks that lack the Eu-anomalies still show strong Sr depletion, which is another indicator of fractionation of plagioclase (e.g., Vander Auwera et al., 1998). As is discussed above, many of these monzodioritic rocks may also contain cumulate plagioclase and that would affect the compositions of whole-rock analysis of such rocks, which could also lead to diminished Eu-anomalies.

The variation of monzodioritic compositions in different suites most likely also reflects the differences in parental magma compositions and the modes of the whole-rocks that were analyzed. Emplacement level might play a role as well and can be further investigated by examining pressure constraints from other phases such as clinopyroxene. These results also highlight the critical importance of publishing modes for all of the massif-type anorthosite suites. The monzodioritic data from intrusions in Norway show more evolved compositions compared to the other suites (Ahvenisto, Laramie, Korosten, and Adirondacks; Fig. 9), and whereas the monzodioritic data from the other suites exhibit decreasing Al_2O_3 content with decreasing Mg#, the more evolved Norway samples (Mg# < 40) show increasing Al_2O_3 with decreasing Mg#. Importantly, also the modeled melts show a slight inflection toward increasing Al_2O_3 content between Mg# ~35–25.

4.3. Origin of the anorthosites: Cumulate compositions, sinking of mafic cumulates, and flotation of plagioclase

The modal amount of plagioclase in the iFC models is lower (40–60 wt%) compared to what is observed from natural anorthositic cumulates (65–90 vol%), but the range of An contents (20–80) is within the range in anorthositic rocks (An30–90; Ashwal and Bybee, 2017 and references therein). The amount of clinopyroxene is higher in the iFC models compared to natural samples, and usually the more common pyroxene to crystallize in the anorthositic rocks is orthopyroxene (Ashwal and Bybee, 2017). Experimental work suggests that basaltic magmas crystallize a maximum of 50–60 vol% plagioclase in the crystallizing assemblage at high pressures (Müntener and Ulmer, 2006). Massif-type anorthosites usually contain 10–15 vol% of mafic minerals (Bybee et al., 2014a) and are believed to lack 30–40 vol% of mafic cumulates crystallized from the basaltic parental magmas (e.g., Charlier et al., 2010; Emslie et al., 1994). The work of Arndt and Goldstein (1989) has shown that when mafic magmas pond, crystallize, and assimilate lower crustal material, the crystallizing mafic phases would sink back into the mantle due to their negative buoyancy. Our MCS-iFC models show that the mafic phases are denser and plagioclase less dense compared to the melt (Fig. 10), suggesting that the mafic cumulates would sink and plagioclase float, which is in line with previous observations (e.g., Bybee et al., 2014a).

When the compositions of modeled cumulates with similar phase assemblages are compared to natural anorthositic cumulates, the modeled cumulates show, for example, lower Al_2O_3 and higher FeO^{tot} but similar CaO compared to natural samples (Figs. 6 and 7). MCS in itself does not take into account sinking or flotation of the solid phases, which would be plausible based on the aforementioned density differences. If the hypothesis that at least some of the mafic cumulates sink is
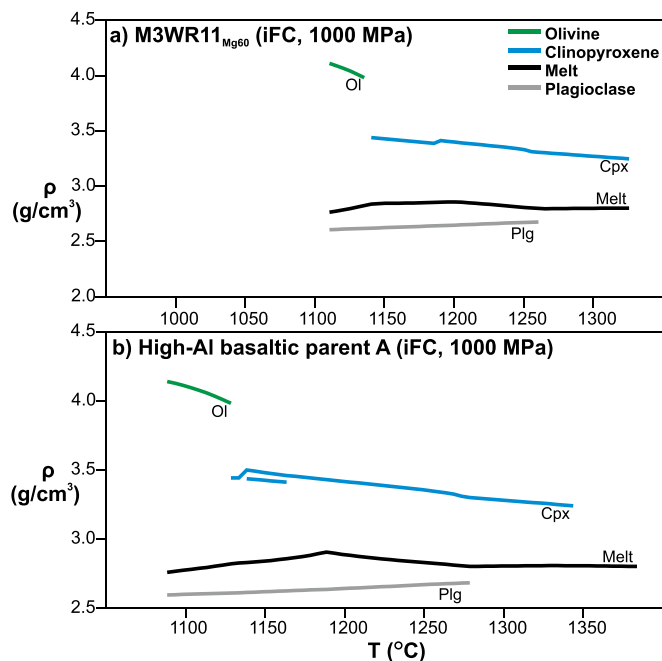
Fig. 10. Examples of density differences between phases (melt, plagioclase, clinopyroxene, and olivine) in iFC simulations at 1000 MPa using a) model melt M3WR11Mg60 and b) high-Al basaltic parent A. Abbreviations are Ol = olivine, Cpx = clinopyroxene, and Plg = plagioclase. See section 4.3 for details.

correct, then the amount of plagioclase relative to the mafic phases increases, leading to relatively higher Al_2O_3 and lower FeO^{tot} contents and possibly yielding a better fit between the modeled cumulate compositions and the natural anorthosite samples. A recent study suggests that plagioclase floats more easily than previously thought (Krättli and Schmidt, 2021). Another explanation for the mismatch between the observed and modeled cumulate compositions may be the limitations of rhyolite-MELTS to accurately model plagioclase crystallization in these kinds of melts (see section 4.4). For example, the incremental cumulate compositions of M3WR11Mg60-iFC show lower Al_2O_3, CaO, and Na_2O and higher FeO^{tot} compared to natural anorthositic rocks (Fig. 6). This could reflect the issue that plagioclase is not the liquidus phase as would be expected in anorthositic rocks, and hence more effective crystallization of clinopyroxene leads to enrichment of FeO^{tot} and depletion of Al_2O_3 and Na_2O in the cumulates.

Further crustal contamination of the parental magmas could also increase plagioclase stability by increasing the Al_2O_3, Na_2O, and SiO_2 contents of the magma (Ashwal, 1993). It has also been suggested that crustal assimilation combined with magma replenishment could enhance plagioclase saturation and lead to production of intermediate plagioclase compositions (Ashwal, 1993). This could also enhance crystallization of orthopyroxene that is known to crystallize from anorthosite parental magmas (e.g., Ashwal and Bybee, 2017), but is only a minor phase in our models. Isotopic evidence of gabbroic and anorthositic rocks in AMCG suites suggests that the high-Al gabbroic rocks show less-contaminated signatures compared to anorthositic rocks (He et al., 2021), indicating that assimilation has also occurred after the massif-type parental magmas of high-Al basaltic compositions were formed. Detailed modeling of this process is outside of the scope of this study, but we encourage future endeavors in this matter.

Finally, based on previous work (e.g., Emslie, 1978; Emslie et al., 1994) and our results we present the following general model for the petrogenesis of massif-type anorthosites (Fig. 11). First (stage 1), mantle-derived partial melts ponded at the crustal-mantle boundary (at ~1000 MPa) and started to crystallize. The heat derived from crystallizing mantle-derived magmas partially melted the surrounding mafic
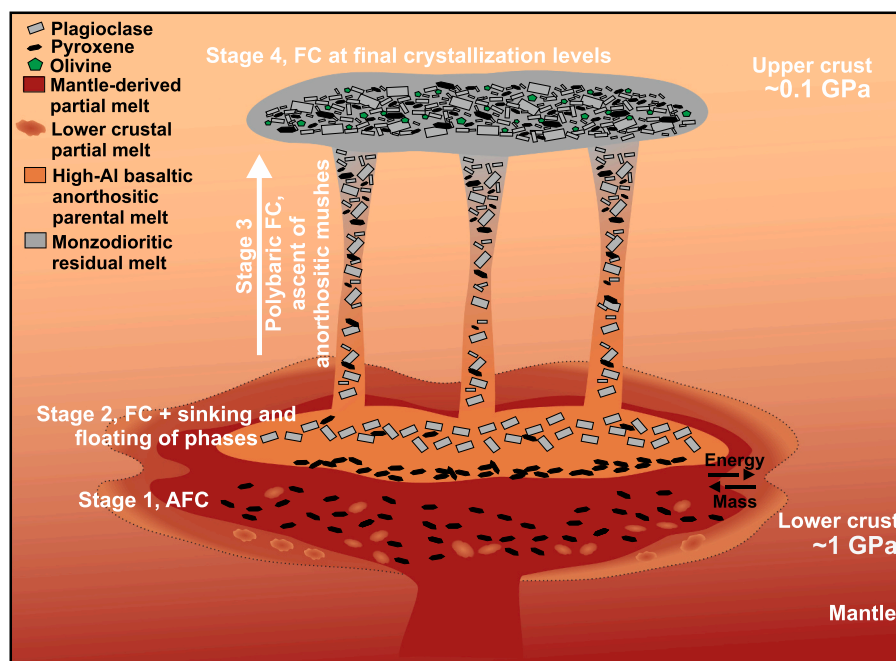
Fig. 11. A schematic petrogenetic model for massif-type anorthosites including four stages: 1) AFC at crust-mantle-boundary, 2) FC at ~1000 MPa and sinking of mafic phases and floating of plagioclase, 3) polybaric FC and ascent of anorthositic mushes through the crust, and 4) final FC of the anorthositic rocks and EC of the monzodioritic residual melts (see Fred et al., 2020) at emplacement levels in the upper crust. See section 4.3 for details.

lower crust, and the produced crustal partial melts were mixed with the mantle-derived magmas (the MCS-AFC models). This AFC led to the production of high-Al basaltic massif-type anorthosite parental melts. Next (stage 2), the basaltic parental melts started to crystallize (FC at ~1000 MPa) and due to density differences, crystallizing mafic phases sank and plagioclase floated producing anorthositic mushes (the iFC models). These mushes then rose through the crust while crystallizing polybarically (stage 3) leaving behind residual melts of monzodioritic composition (the pFC models). The fractional crystallization (stage 4) of the anorthositic rocks occurred at final emplacement levels in the upper crust (~300–200 MPa) and was accompanied by equilibrium crystallization of the monzodioritic residual melts (see Fred et al., 2020).

4.4. Model limitations and future prospects

As with all models, MELTS and MCS have their limitations. One possible issue in the presented models might be delayed crystallization of plagioclase at high pressures, which has also been observed to be an issue in some other studies (see Fred et al., 2020; Putirka, 2005). This might play a role in the minor mismatch of the model results with natural data, but as discussed in section 4.3, there are also other potential explanations for this mismatch. Also, rhyolite-MELTS is built on collected data of thermodynamic models for silicate liquid, mineral, and fluid phases, with the liquid-phase properties derived partly from experimental liquid-solid phase equilibrium data and, hence it is affected by limitations of incomplete data coverage, inconsistent data, and inadequacies of the thermodynamic solution theory (Ghiorso and Gualda, 2015). The peculiar compositions of the high-aluminum orthopyroxene megacrysts typical to massif-type anorthsites are not incorporated in the MELTS database, and thus might raise concerns about the suitability of the used tools to model massif-type anorthosite petrogenesis. Rhyolite-MELTS, however, is able to incorporate several weight percents of Al_2O_3 in the crystallizing orthopyroxene in our MCS-AFC models. Hence, we consider the use of rhyolite-MELTS and MCS justified for the purpose, although highest Al_2O_3 content found in natural orthopyroxene megacrysts (up to 9 wt%) are not produced by the models.

As mentioned in section 4.3, assimilation of lower crustal material by massif-type anorthosite parental magmas could lead to enhanced stabilization of plagioclase. Since the MCS can model simultaneous recharge-assimilation-fractional crystallization (RAFC) processes, one of the future prospects would be to use MCS to study the effect of crustal assimilation of the anorthosite parental magmas combined with magma recharge to investigate if added crustal mass would address the differences in the modes (e.g., plagioclase-clinopyroxene-ratio) and the associated mismatch of modeled versus observed compositions.

The goals of our modeling were to test the suitability of the used modeling tools and to investigate the broad spectrum of processes that contribute to the petrogenesis of massif-type anorthosites. The model outcomes support the four-stage petrogenetic model presented (Fig. 11). In this study, we used major element and phase equilibria data and focused on AFC and FC processes. However, several of the hypotheses for the petrogenesis of massif-type anorthosites base their arguments on isotopic compositions (e.g., mantle vs. crustal source) of individual suites (e.g., Schiellerup et al., 2000). The success of the modeling we have done strongly implies that more detailed thermodynamic and geochemical modeling, including the addition of suite-specific trace element and isotope data, could be used to study the petrogenesis of individual massif-type anorthosite suites as well as other igneous suites. We strongly recommend such modeling in the future. For example, crystallization of apatite plays an important role especially in the evolution of the most evolved monzodioritic rocks and has a significant effect on the trace element compositions. P_2O_5 is not included in our models due to lack of data for some of the used starting compositions. Preliminary test simulations show that addition of P_2O_5 has only minor effect on the main outcomes of our models. Nevertheless, it is clear that P_2O_5 needs to incorporated in future modeling of individual intrusions when trace elements are considered.

Assimilation plays an important role in anorthosite petrogenesis, and for example in the Voisey's Bay Intrusions in Nain Plutonic Suite, the crucial factor leading to sulfide saturation is the composition of the assimilant, which is a sulfide-bearing gneissic rock (e.g., Li et al., 2000). Combined with a suitable sulfide saturation model, MCS could also be used to study ore-forming processes in massif-type anorthosites. Sulfide

saturation might be a more common process during massif-type anorthosites than is generally assumed (Hannah and Stein, 2002). Cumulate rocks with anomalous compositions, such as the Fe-Ti-P-enriched oxide-apatite-gabbronorites (OAGNs) and nelsonites (Dymek and Owens, 2001) have also been reported to occur in massif-type anorthosite suites. The incremental cumulate compositions of our models (Supplementary material F) suggest that similar anomalous low Si (~30 wt%) and high Fe (>30 wt%) and Ti (>10 wt%) can be produced by fractional crystallization of massif-type anorthosite parental magmas. MCS could, therefore, also be used to study the crystallization of these peculiar cumulates.

5. Conclusions

The results of this study are promising, and the following outcomes are, thus, proposed, with the caveat that all models have limitations, and model outcomes should be used to inform addiotional hypotheses testing. Our petrological modeling suggest that massif-type anorthosite high-Al basaltic parental magmas were generated when hot, primitive, mantle-derived magmas assimilated mafic lower crustal material at Moho depths. In contrast, the production of the parental melts by directly melting the lower crust requires the crust to melt to a high degree or completely (>70 wt%), which would destabilize the crust and would be impossible without associated mantle magmatism. Our models do not support the suggestion that the monzodioritic rocks are parental to anorthosites. Instead, fractional crystallization of the high-Al basaltic parental melts produce similar LLDs to the general evolutionary trend of the monzodioritic rocks, suggesting that the monzodioritic rocks most likely represent the residual melts after fractional crystallization. Anorthosites represent selective cumulates from this fractionating process; that is, density separation of mafic phases (i.e. sinking) and plagioclase (i.e. floating) are suggested to produce the high plagioclase mode of the anorthosites. We link our modeling to a four-stage petrogenetic model for the massif-type anorthosites: 1) AFC at Moho levels producing high-Al basaltic anorthosite parental magmas, 2) high-pressure FC of the anorthosite parental magmas and sinking of mafic phases and plagioclase flotation, 3) polybaric FC of the ascending plagioclase-rich mushes, and 4) low-pressure crystallization of the anorthositic cumulates and monzodioritic residual melts. Our results suggest that this four-stage model quite well represents the general process for the evolution of massif-type anorthosite suites and can be used as framework for more detailed modeling of individual suites with MCS and rhyolite-MELTS tools in the future.

Declaration of Competing Interest

The authors declare that they have no known competing financial interests or personal relationships that could have appeared to influence the work reported in this paper.

Appendix A. Supplementary data

Supplementary data to this article can be found online at https://doi.org/10.1016/j.lithos.2022.106751.

References

Arndt, N.T., Goldstein, S.L., 1989. An open boundary between lower continental crust and mantle: Its role in crust formation and recycling. In: Ashwal, L.D. (Ed.), Growth of the Continental Crust, Tectonophysics, vol. 161, pp. 201–212.

Ashwal, L.D., 1982. Mineralogy of mafic and Fe-Ti oxide-rich differentiates of the Marcy anorthosite massif, Adirondack, New York. Am. Mineral. 67, 14–27.

Ashwal, L.D., 1993. Anorthosites. Minerals and Rocks 21. Springer-Verlag, Berlin, Heidelberg, p. 422.

Ashwal, L.D., Bybee, G.M., 2017. Crustal evolution and temporality of anorthosites. Earth Sci. Rev. 173, 307–330. https://doi.org/10.1016/j.earscirev.2017.09.002.

Bohrson, W.A., Spera, F.J., 2001. Energy-constrained open-system magmatic processes II: application of energy-constrained assimilation-fractional crystallization (EC-AFC) model to magmatic systems. J. Petrol. 42, 1019–1041. https://doi.org/10.1093/petrology/42.5.1019.

Bohrson, W.A., Spera, F.J., 2007. Energy-constrained recharge, assimilation, and fractional crystallization (EC-RAXFC): a visual basic computer code for calculating trace element and isotope variations of open-system magmatic systems. Geochem. Geophys. Geosyst. 8, Q11003. https://doi.org/10.1029/2007G C001781.

Bohrson, W.A., Spera, F.J., Ghiorso, M.S., Brown, G.A., Creamer, J.B., Mayfield, A., 2014. Thermodynamic models for energy-constrained open-system evolution of crustal magma bodies undergoing simultaneous recharge, assimilation and crystallization: the Magma Chamber Simulator. J. Petrol. 55, 1685–1717. https://doi.org/10.1093/petrology/egu036.

Bohrson, W.A., Spera, F.J., Heinonen, J.S., Brown, G.A., Scruggs, M.A., Adams, J.V., Takach, M.K., Zeff, G., Suikkanen, E., 2020. Diagnosing open-system magmatic processes using the Magma Chamber Simultaor (MCS): part I – major elements and phase equilibria. Contrib. Mineral. Petrol. 175 https://doi.org/10.1007/s00410-020-01722-z.

Borisova, A.Y., Bohrson, W.A., Grégoire, M., 2017. Origin of primitive ocean island basalts by crustal gabbro assimilation and multiple recharge of plume-derived melts. Geochem. Geophys. Geosyst. 18, 2701–2716. https://doi.org/10.1002/2017GC006986.

Bowen, N.L., 1917. The problem of the anorthosites. J. Geol. 25, 209–243.

Bybee, G.M., Ashwal, L.D., Shirey, S.B., Horan, M., Mock, T., Andersen, T.B., 2014a. Pyroxene megacrysts in Proterozoic anorthosites: Implications for tectonic setting, magma source and magmatic processes at the Moho. Earth Planet. Sci. Lett. 389, 74–85. https://doi.org/10.1016/j.epsl.2013.12.015.

Bybee, G.M., Ashwal, L.D., Shirey, S.B., Horan, M., Mock, T., Andersen, T.B., 2014b. Debating the petrogenesis of Proterozoic anorthosites–reply to comments by Vander Auwera et al. on 'pyroxene megacrysts in Proterozoic anorthosites: implications for tectonic setting, magma source and magmatic processes at the Moho'. Earth Planet. Sci. Lett. 401, 381–383. https://doi.org/10.1016/j.epsl.2014.06.032.

Bybee, G.M., Ashwal, L.D., Gover, C.F., Hamilton, M.A., 2015. Pegmatitic pods in the mealy mountains intrusive suite, Canada: clues to the origin of the olivine-orthopyroxene dichtomy in proterozoic anorthosites. J. Petrol. 56, 845–868. https://doi.org/10.1093/petrology/egv019.

Charlier, B., Duchesne, J.C., Vander Auwera, J., Storme, J.Y., Maquil, R., Longhi, J., 2010. Polybaric fractional crystallization of high-alumina basalt parental magmas in the egersund-ogna massif-type aorthosite (Rogaland, SW Norway) constrained by plagioclase and high-alumina orthopyroxene megacrysts. J. Petrol. 51 (12), 2515–2546. https://doi.org/10.1093/petrology/egq066.

Coltice, N., Phillips, B.R., Bertrand, H., Ricard, Y., Rey, P., 2007. Global warming of the mantle at the origin of flood basalts over supercontinents. Geology 35, 391–394. https://doi.org/10.1016/j.gr.2008.10.001.

Coltice, N., Bertrand, H., Rey, P., Jourdan, F., Phillips, B.R., Ricard, Y., 2009. Global warming of the mantle beneath continents back to the Archean. Gondwana Res. 15, 254–266. https://doi.org/10.1130/G23240A.1.

Condie, K.C., Selverstone, J., 1999. The crust of the Colorado plateau: new views of an old arc. J. Geol. 107 (4), 387–397. https://doi.org/10.1086/314363.

Demaiffe, D., Hertogen, J., 1981. Rare-earth element geochemistry and strontium isotopic composition of a massif-type anorthositic-charnokitic body: the Hidra Massif (Rogaland, SW Norway). Geochem. Cosmochim. Acta 45, 1545–1561. https://doi.org/10.1016/0016-7037(81)90284-2.

DePaolo, D.J., 1981. Trace element and isotopic effects of combined wallrock assimilation and fractional crystallization. Earth Planet. Sci. Lett. 53, 189–202. https://doi.org/10.1016/0012-821x(81)90153 -9.

Duchesne, J.C., 1984. Massif anorthosites: another partisan review. Feldspars and Felspathoids. NATO Advanced Study Institute C137, 411–433.

Duchesne, J.C., Demaiffe, D., 1978. Trace elements and anorthosite genesis. Earth Planet. Sci. Lett. 38, 249–272.

Duchesne, J.C., Hertogen, J., 1988. Le Magma Parental du Lopolithe de Bjerkreim-Sokndal (Norvege meridionale).

Duchesne, J.C., Liégeois, J.P., Vander Auwera, J., Longhi, J., 1999. The crustal tongue melting model and the origin of massive anorthosites. Terra Nova 11, 100–105. https://doi.org/10.1046/j.1365-3121.1999.00232.x.

Duchesne, J.C., Roelandts, I., Demaiffe, D., Hertogen, J., Gibjels, R., De Winter, J., 1974. Rare-earth data on monzonoritic rocks related to anorthosites and their bearing on the nature of the parental magma of the anorthositic series. Earth Planet. Sci. Lett. 24, 325–335. https://doi.org/10.1016/0012-821X(74)90112-5.

Duchesne, J.C., Shumlyanskyy, L., Mytrokhyn, O.V., 2017. The jotunite of the Korosten AMCG complex (Ukranian shield): Crust- or mantle-derived? Precambrian Res. 299, 58–74. https://doi.org/10.1016/j.precamres.2017.07.018.

Dymek, R.F., Owens, B.E., 2001. Petrogenesis of Apatite-Rich Rocks (Nelsonites and Oxide-Apatite Gabbronorites) Associated with Massif Anorthosites. Econ. Geol. 96, 797–815. https://doi.org/10.2113/gsecongeo.96.4.797.

Emslie, R.F., 1978. Anorthosite massifs, rapakivi granites, and late Proterozoic rifting of North America. Precambrian Res. 64, 273–288. https://doi.org/10.1016/0301-9268 (78)90005-0.

Emslie, R.F., Hamilton, M.A., Thériault, R.J., 1994. Petrogenesis of a Mid-Proterozoic anorthosite-mangerite-charnockite-granite (AMCG) complex: isotope and geochemical evidence from the Nain Plutonic suite. J. Geol. 102, 539–558. https://doi.org/10.1086/629697.

Fowler, S.J., Bohrson, W.A., Spera, F.J., 2004. Magmatic evolution of the Skye Igneous Centre, Western Scotland: modelling of assimilation, recharge and fractional crystallization. J. Petrol. 45, 2481–2505. https://doi.org/10.1093/petrology/egh074.

Fred, R., Heinonen, A., Heinonen, J.S., 2020. Equilibrium crystallization of massif-type anorthosite residual melts: a case study from the 1.64 Ga Ahvenisto complex, Southeastern Finland. Contrib. Mineral. Petrol. 75, 86. https://doi.org/10.1007/s00410-020-01726-9.

Frost, C.D., Frost, B.R., 1997. Reduced rapakivi-type granites: the tholeiite connection. Geology 25, 647–650. https://doi.org/10.1130/0091-7613(1997)025<0647:RRTGTT>2.3.CO;2.

Ganne, J., Feng, X., 2017. Primary magmas and mantle temperatures through time. Geochem. Geophys. Geosyst. 18, 872–888. https://doi.org/10.1002/2016GC006787.

Gao, S., Zhang, B.-R., Jin, Z.-M., Kern, H., Luo, T.-C., Zhao, Z.-D., 1998. How mafic is the lower continental crust? Earth Planet. Sci. Lett. 106, 101–117. https://doi.org/10.1016/S0012-821X(98)00140-X.

Ghiorso, M.S., Sack, R.O., 1995. Chemical mass transfer in magmatic processes IV. A revised and internally consistent thermodynamic model for the interpolation and extrapolation of liquid-solid equilibria in magmatic systems at elevated temperatures and pressures. Contrib. Mineral. Petrol. 119, 197–212. https://doi.org/10.1007/BF00307281.

Ghiorso, M.S., Gualda, G.A.R., 2015. Chapter 6 - Chemical Thermodynamics and the Study of Magmas. In: Sigurdsson, Haraldur (Ed.), The Encyclopedia of Volcanoes, Second edition. Academic Press, pp. 143–161. https://doi.org/10.1016/B978-0-12-385938-9.00006-7.

Gualda, G.A.R., Ghiorso, M.S., Lemons, R.V., Carley, T.L., 2012. Rhyolite-MELTS: a Modified Calibration of MELTS optimized for Silica-rich, Fluid-bearing Magmatic Systems. J. Petrol. 53, 875–890. https://doi.org/10.1093/petrology/egr080.

Hannah, J.L., Stein, H.J., 2002. Re-Os model for the origin of sulfide deposits in anorthosite-associated intrusive complexes. Econ. Geol. 97, 371–383. https://doi.org/10.2113/gsecongeo.97.2.371.

He, H.-L., Zhai, M.-G., Lu, J.-S., Zhao, Y., Zhang, C.-L., George, Sajeev, P.M., Rajkumar, K.P., Gou, L.-L., Ao, W.-H., Hu, Y.-H., 2021. Lower crust-mantle interactions in the massif-type anorthosite formation: New evidence from zircon U-Pb-Hf-O isotopes of the Neoproterozoic Kadavur complex, southern India. Lithos 380–381. https://doi.org/10.1016/j.lithos.2020.105836.

Heinonen, A., Rämö, O.T., Mänttäri, I., Johanson, B., Alviola, R., 2010. Formation and fractionation of High-Al tholeiitic magmas in the Ahvenisto rapakivi granite–massif-type anorthosite complex, southeastern Finland. Can. Mineral. 48, 969–990. https://doi.org/10.3749/canmin.48.4.969.

Heinonen, A., Andersen, T., Rämö, O.T., Whitehouse, M.J., 2015. The source of Proterozoic anorthosite and rapakivi granite magmatism: evidence from combined *in situ* Hf-O isotopes of zircon in the Ahvenisto complex, southeastern Finland. J. Geol. Soc. 172, 103–112. https://doi.org/10.1144/jgs2014-013.

Heinonen, A., Kivisaari, H., Michallik, R.M., 2020. High-aluminum orthopyroxene megacrysts (HAOM) in the Ahvenisto complex, SE Finland, and the polybaric crystallization of massif-type anorthosites. Contrib. Mineral. Petrol. 175, 10. https://doi.org/10.1007/s00410-019-1648-5.

Heinonen, J.S., Luttinen, A.V., Bohrson, W.A., 2016. Enriched continental flood basalts from depleted mantle melts: modeling the lithospheric contamination of Karoo lavas from Antarctica. Contrib. Mineral. Petrol. 171 https://doi.org/10.1007/s0041 0-015-1214-8.

Heinonen, J.S., Luttinen, A.V., Spera, F.J., Bohrson, W.A., 2019. Deep open storage and shallow closed transport system for a continental flood basalt sequence revealed with Magma Chamber Simulator. Contrib. Mineral. Petrol. 174 https://doi.org/10.1007/s00410-019-1624-0.

Heinonen, J.S., Iles, K.A., Heinonen, A., Fred, R., Virtanen, V.J., Bohrson, W.A., Spera, F.J., 2021. From binary mixing to magma chamber simulator. Crus. Magmatic Evol. https://doi.org/10.1002/9781119564485.ch7.

Heinonen, J.S., Spera, F.J., Bohrson, W.A., 2022. Thermodynamic limits for assimilation of silicate crust in primitive magmas. Geology. https://doi.org/10.1130/G49139.1 in press.

Iles, K.A., Heinonen, J.S., 2022. Modelling the formation of linear geochemical trends using the Magma Chamber Simulator: a case study of the Jindabyne Granitoids, Lachlan Fold Belt, Australia. J. Petrol. 63 https://doi.org/10.1093/petrology/egab102.

Kiefer, W.S., Filiberto, J., Sandu, C., Li, Q., 2015. The effects of mantle composition on the peridotite solidus: Implications for the magmatic history of Mars. Geochim. Cosmochim. Acta 162, 247–258. https://doi.org/10.1016/j.gca.2015.02.010.

Krättli, G., Schmidt, M.W., 2021. Experimental settling, flotation and compaction of plagioclase in basaltic melt and a revision of melt density. Contrib. Mineral. Petrol. 176 https://doi.org/10.1007/s00410-021-01785-6.

Kärenlampi, K., Heinonen, J.S., Kontinen, A., Hanski, E., Huhma, H., 2021. Geochemical and thermodynamic modeling of the petrogenesis of A1-type granites and associated intermediate rocks: a case study from the central Fennoscandian Shield. Geochemistry. https://doi.org/10.1016/j.chemer.2020.125734 in press.

Li, C., Lightfoot, P.C., Amelin, Y., Naldrett, A.J., 2000. Contrasting petrological and geochemical relationships in the voisey's Bay and Mushuau Intrusions, Labrador,

Canada: implications for ore genesis. Econ. Geol. 95, 771–799. https://doi.org/10.2113/gsecongeo.95.4.771.

Liu, Y.S., Gao, S., Jin, S.Y., Hu, S.H., Sun, M., Zhao, Z.B., Feng, J.L., 2001. Geochemistry of lower crustal xenoliths from Neogene Hannuoba basalt, North China craton: implications for petrogenesis and lower crustal composition. Geochim. Cosmochim. Acta 65 (15), 2589–2604. https://doi.org/10.1016/S0016-7037(01)00609-3.

Longhi, J., 2005. A mantle or mafic crustal source for Proterozoic anorthosites? Lithos 83, 183–198. https://doi.org/10.1016/j.lithos.2005.03.009.

Longhi, J., Vander Auwera, J., Fram, M.S., Duchesne, J.-C., 1999. Some phase equilibrium constraints on the origin of Proterozoic (Massif) anorthosites and related rocks. J. Petrol. 40, 339–362. https://doi.org/10.1093/petroj/40.2.339.

Markl, G., 2001. REE constraints on fractionation processes of massif-type anorthosites on the Lofoten Islands, Norway. Mineral. Petrol. 72, 325–351. https://doi.org/10.1007/s007100170022.

McLelland, J., Ashwal, L., Moore, L., 1994. Composition and petrogenesis of oxide-, apatite-rich gabbronorites associated with Proterozoic anorthosite massifs: examples from the Adirondack Mountains, New York. Contrib. Mineral. Petrol. 116, 225–238. https://doi.org/10.1007/BF00310702.

Mitchell, J.N., Scoates, J.S., Frost, C.D., 1995. High-Al gabbros in the Laramie Anorthosite complex, Wyoming: implications for the composition of melts parental to Proterozoic anorthosite. Contrib. Mineral. Petrol. 119, 166–180. https://doi.org/10.1007/BF00307279.

Mitchell, J.N., Scoates, J.S., Frost, C.D., Kolker, A., 1996. The geochemical evolution of anorthosite residual magmas in the Laramie Anorthosite Complex, Wyoming. J. Petrol. 37, 637–660. https://doi.org/10.1093/petrology/37.3.637.

Moore, N.E., Grunder, A.L., Bohrson, W.A., 2018. The three-stage petrochemical evolution of the Steens Basalt compared to large igneous provinces and layered mafic intrusions. Geosphere 14, 2505–2532. https://doi.org/10.1130/GES01665.1.

Morisset, C.-E., Scoates, J.S., Weis, D., Friedman, R.M., 2009. U–Pb and 40Ar/39Ar geochronology of the Saint-Urbain and Lac Allard (Havre-Saint-Pierre) anorthosites and their associated Fe–Ti oxide ores, Québec: Evidence for emplacement and slow cooling during the collisional Ottawa orogeny in the Grenville Province. Precambrian Res. 174, 95–116. https://doi.org/10.1016/j.precamres.2009.06.009.

Morse, S.A., 1982. A partisan review of Proterozoic anorthosites. Am. Mineral. 67, 1087–1100.

Mukherjee, A., Das, S., 2002. Anorthosites, Granulites and the Supercontinent Cycle. Gondwana Res. 5, 147–156. https://doi.org/10.1016/S1342-937X(05)70898-4.

Müntener, O., Ulmer, P., 2006. Experimentally derived high-pressure cumulates from hydrous arc magmas and consequences for the seismic velocity structure of lower arc crust. Geophys. Res. Lett. 33, L21308. https://doi.org/10.1029/2006GL027629.

Owens, B.E., Dymek, R.F., 1992. Fe-Ti-P-rich rocks and massif anorthosite; problems of interpretation illustrated from the Labrieville and St-Urbain plutons, Quebec. Can. Mineral. 30, 163–190.

Owens, B.E., Rockow, M.W., Dymek, R.F., 1993. Jotunites from the Grenville Province, Quebec: petrological characteristics and implications for massif anorthosite petrogenesis. Lithos 30, 57–80.

Putirka, K.D., 2005. Igneous thermometers and barometers based on plagioclase + liquid equilibria: Test of some existing models and new calibrations. Am. Mineral. 90, 336–346. https://doi.org/10.2138/am.2005.1449.

Rudnick, R.L., Fountain, D.M., 1995. Nature and composition of the continental crust: a lower crustal perspective. Rev. Geophys. 33 (3), 267–309. https://doi.org/10.1029/95RG01302.

Rudnick, R.L., Presper, T., 1990. Geochemistry of intermediate to high-pressure granulites. In: Vielzeuf, D., Vidal, P. (Eds.), Granulites and Crustal Evolution, pp. 523–550. https://doi.org/10.1007/978-94-009-2055-2_27. Kluwer, Amsterdam.

Rudnick, R.L., Taylor, S.R., 1987. The composition and petrogenesis of the lower crust: a xenolith study. J. Geophys. Res. 92 (B13), 13981–14005. https://doi.org/10.1029/JB092iB13p13981.

Schiellerup, H., Lambert, D.D., Prestvik, T., Robins, B., McBride, J.S., Larsen, R.B., 2000. Re-Os isotopic evidence for a lower crustal origin of massif-type anorthosites. Nature 405, 781–784. https://doi.org/10.1038/35015546.

Schärer, U., Wilmart, E., Duchesne, J.-C., 1996. The short duration and anorogenic character of anorthosite magmatism: U-Pb dating of the Rogaland complex, Norway. Earth Planet. Sci. Lett. 139, 335–350. https://doi.org/10.1016/0012-821X(96)00033-7.

Seifert, K.E., Dymek, R.F., Whitney, P.R., Haskin, L.A., 2010. Geochemistry of massif anorthosite and associated rocks, Adirondacks Mountains , New York. Geosphere 6, 855–899. https://doi.org/10.1130/GES00550.1.

Shaw, D.M., Dickin, A.P., Li, H., McNutt, R.H., Schwarcz, H.P., Truscott, M.G., 1994. Crustal geochemistry in the Wawa-Foleyet region, Ontario. Can. J. Earth Sci. 31 (7), 1104–1121. https://doi.org/10.1139/e94-099.

Spera, F.J., Bohrson, W.A., 2001. Energy-constrained open-system magmatic processes I: general model and energy-constrained assimilation and fractional crystallization (EC-AFC) formulation. J. Petrol. 42, 999–1018. https://doi.org/10.1093/petrology/42.5.999.

Takahashi, E., 1986. Melting of a Dry Peridotite KLB-1 up to 14 GPa: Implications on the Origin of Peridotitic Upper Mantle. J. Geophys. Res. 91, 9367–9382. https://doi.org/10.1029/JB091iB09p09367.

Taylor, H.P., 1980. The effects of assimilation of country rocks by magmas on 18O/16O and 87Sr/86Sr systematics in igneous rocks. Earth Planet. Sci. Lett. 47, 243–254. https://doi.org/10.1016/0012-821X(80)90040-0.

Taylor, S.R., McLennan, S.M., 1985. The Continental Crust: Its Composition and Evolution. Blackwell, Oxford.

Taylor, S.R., McLennan, S.M., 1995. The geochemical evolution of the continental crust. Rev. Geophys. 33, 241–265. https://doi.org/10.1029/95RG00262.

Vander Auwera, J., Longhi, J., Duchesne, J.C., 1998. A Liquid Line of decent of the Jotunite (Hypersthene Monzodiorite) Suite. J. Petrol. 39, 439–468. https://doi.org/10.1093/petroj/39.3.439.

Villaseca, C., Downes, H., Pin, C., Barbero, L., 1999. Nature and composition of the lower continental crust in Central Spain and the granulite-granite linkage: inferences from granulitic xenoliths. J. Petrol. 40 (10), 1465–1496. https://doi.org/10.1093/petroj/40.10.1465.

Weaver, B.L., Tarney, J., 1984. Empirical approach to estimating the composition of the continental crust. Nature 310, 575–577. https://doi.org/10.1038/310575a0.

Walter, M.J., 1998. Melting of Garnet Peridotite and the Origin of Komatiite and Depleted Lithosphere. J. Petrol. 39, 29–60. https://doi.org/10.1093/petroj/39.1.29.

Wedepohl, H., 1995. The composition of the continental crust. Geochim. Cosmochim. Acta 59, 1217–1239. https://doi.org/10.1016/0016-7037(95)00038-2.